Nuclear-spin relaxation in molecular solids with reorienting methyl and *t*-butyl groups: The spectral density and the state of the solid

Peter A. Beckmann, Audrey I. Hill, Ellen B. Kohler, and Hong Yu
Department of Physics, Bryn Mawr College, Bryn Mawr, Pennsylvania 19010
(Received 24 August 1987; revised manuscript received 23 March 1988)

We have measured the temperature T dependence of the proton Zeeman relaxation rate R in polycrystalline 1,3-di-*t*-butylbenzene (1,3-DTB) at Larmor frequencies of $\omega/(2\pi)=8.50$, 22.5, and 53.0 MHz. The relaxation is caused by the modulation of the methyl proton dipole-dipole interactions by the reorientation of the *t*-butyl groups [$C(CH_3)_3$] and their three constituent methyl groups (CH_3). There are two solid phases which either have a large hysteresis of at least 90 K, or are both stable below 200 K. The sample melts at 262 K. We interpret the high-temperature phase R-versus-T^{-1} data with three models. First, we adopt a one-correlation-time model using a Davidson-Cole spectral density which suggests that there is a distribution of correlation times, or, equivalently, a distribution of activation energies for *t*-butyl and methyl group reorientation. In this case, the methyl and *t*-butyl reorientation is characterized by a cutoff activation energy of 17 ± 1 kJ/mol which is to be compared with 18 ± 1 kJ/mol in 1,4-DTB [P. A. Beckmann, F. A. Fusco, and A. E. O'Neill, J. Magn. Reson. **59**, 63 (1984)] in which there is only the one phase. Second, we adopt two two-correlation-time models using Bloembergen-Purcell-Pound spectral densities; one based on the dynamical inequivalence of the methyl groups in each *t*-butyl group and one based on the dynamical inequivalence of different *t*-butyl groups, either because of intramolecular effects or because of intermolecular (crystal-structure) effects. In the low-temperature phase of 1,3-DTB, $R(\omega,T)$ is unusual in that it is Larmor-frequency dependent in the short-correlation-time limit (i.e., temperatures above the relaxation rate maximum). We have fit the data with a Havriliak-Negami spectral density (which reduces to a Davidson-Cole spectral density when one of the parameters becomes unity which, in turn, reduces to a Bloembergen-Purcell-Pound spectral density when an additional parameter becomes unity). The fit, with an effective activation energy of 10 ± 3 kJ/mol, suggests that this low-temperature phase in 1,3-DTB is a glassy state. We relate the Havriliak-Negami spectral density to the Dissado-Hill spectral density which has a fundamental microscopic basis and which has been used to interpret a vast quantity of dielectric relaxation data as well as some mechanical relaxation data.

I. INTRODUCTION

Nuclear-spin relaxation (NSR) is a powerful experimental technique for investigating molecular motion in condensed phases.[1-4] The observed Zeeman nuclear-spin-lattice relaxation rate R is a measure of the rate at which an excited nuclear-spin system returns to equilibrium. When a nuclear spin moves due to whole molecule or intramolecular motion, it creates a time-dependent dipolar magnetic field at the sites of neighboring nuclear spins. A perturbed spin system will relax to its equilibrium state via stimulated emission by sampling the Fourier component of the local time-dependent fields corresponding to the Zeeman splitting. Thus, the observed rate R contains information about the local molecular dynamics. R depends on the Larmor angular frequency ω and the temperature T. The Larmor angular frequency is determined by the applied magnetic field of magnetic field strength B via $\omega=\gamma B$ where γ is the magnetogyric ratio of the nucleus. $R(\omega,T)$ can be modeled in terms of parameters which characterize the structure of the molecule and the solid and by parameters which characterize the anisotropic electrostatic environment in which the motion takes place. This electrostatic potential has both an intramolecular and an intermolecular component and in the solid state their relative importance varies considerably. *t*-butyl groups are relatively large and bulky and the intermolecular potential is usually significant. Since the intermolecular electrostatic environment is usually strongly dependent on the state of the solid, R can be very sensitive, not only to the state itself, but also to changes in state[5-8] even though NSR cannot, in general, determine the structural details. For a given state, the link between R and a local anisotropic electrostatic potential V is an effective correlation time τ that characterizes the time scale over which the local magnetic fields change. The link between τ and V is model dependent, as is the link between T and τ.[9]

The results of NSR experiments are rarely, by themselves, definitive. In addition to detecting changes in state, the technique is very good for determining which motions are occurring in simple systems. The technique is also very good for determining the statistics and the effective parameters that characterize the motion. However, the NSR results must often be coupled with other techniques, such as calorimetry,[10-12] x-ray diffraction,[12-14] and neutron scattering,[11,14-15] to obtain both precise unambiguous models and parameters which

describe the molecular motion, and to be able to say how these parameters relate to the state of the solid. An important avenue of research is to explore the links between the experimental observables (including the model-independent parameters which naturally arise in fitting data) and the theoretical parameters which are most relevant to the fundamental physics.

In this paper we present a proton Zeeman NSR study in an organic molecular solid: the 1,3 isomer of di-*t*-butylbenzene (DTB) which is shown schematically in Fig. 1(b). The motion, depicted schematically in Fig. 2, is that of three methyl groups (CH_3) superimposed on a *t*-butyl group [$C(CH_3)_3$]. $R(\omega,T)$ versus T^{-1} is shown in Fig. 3. These motions are one-dimensional reorientations about (at least) threefold axes determined by an electrostatic potential $V(\phi)$ where ϕ is a rotation angle.[16] One defines a model-dependent reorientation time or correlation time τ to characterize the motion and it typically ranges from $10^{-4}\omega^{-1}$ to $10^{4}\omega^{-1}$ over the temperature range studied here. This is discussed further in Sec. III B. The molecules are chosen such that there are no other motions of the nuclear spins (protons) on the Zeeman nuclear magnetic resonance time scale.

The observed $R(T)$ in polycrystalline 1,4-DTB (Ref. 17) is typical of many simple solids and the models used to fit the data[17,18] suggest that the reorientation process can be described by a simple model which we discuss in more detail in Sec. III C 1. This isomer shows no phase transitions and the structure, although not known, is probably one of a few standard forms.[19] The observed $R(T)$ in the 1,3 isomer, however, shows two phases (Fig. 3) and the $R(\omega,T)$ observed in the high-temperature phase (Figs. 4–7) is very different from that observed in the low-temperature phase (Fig. 8). The observed $R(\omega,T)$ in the high-temperature phase is very similar to that observed over the entire temperature region in the 1,4 isomer.[17] It is not unusual for organic molecular solids to exist in two phases[19] and 1,3 isomers in particular tend to form different states, or have anomalous R-versus-T^{-1} features,[20] or both.[21,22] Both phases can be very stable[19] and which of the two states the sample is in will usually depend on the thermal preparation.[19–22] Of particular note for the low-temperature phase of the 1,3 isomer is the dependence of R on ω at temperatures above the maximum in R (Fig. 8). Usually, R does not depend on ω in this region (e.g., the high-temperature phase in Fig. 5). By using the results from dielectric relaxation (DR) studies, we will suggest below that the low-temperature phase is characteristic of a "glassy" state.

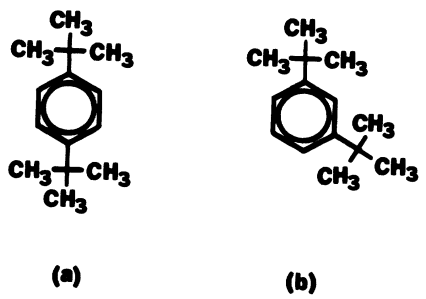

FIG. 1. A schematic representation of the (a) 1,4 and the (b) 1,3 isomers of di-*t*-butylbenzene (DTB). C is carbon, H is hydrogen, and only the atoms in the methyl groups are indicated.

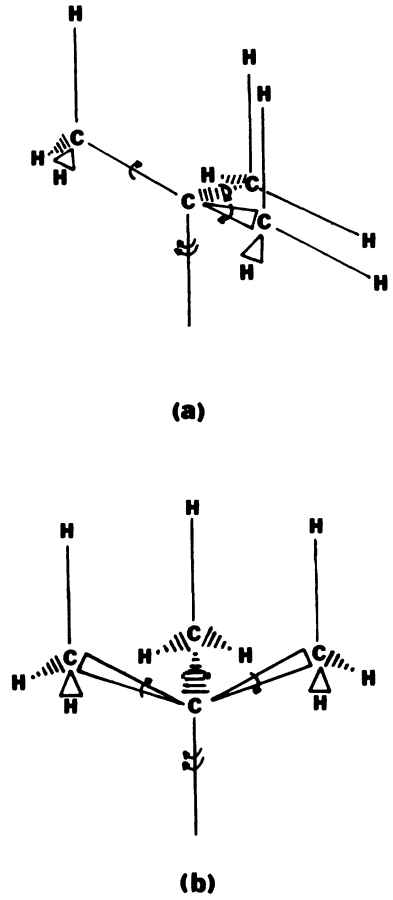

FIG. 2. Two drawings of a tertiarybutyl (*t*-butyl) group showing the position of the three methyl groups. For ring compounds like DTB, the lower vertical bond goes to the carbon atom in the ring. Solid lines represent bonds in a plane parallel to (but not necessarily in) the plane of the page, solid wedges represent bonds where the wide end of the wedge next to an atom is more out of the page than the pointed end next to an atom, and dashed wedges represent bonds where the pointed end of the wedge next to an atom is more into the page than the wide end next to an atom. Methyl reorientation is indicated by single arrows and *t*-butyl reorientation is indicated by a double arrow. Two different perspectives are shown. In (a), the *t*-butyl reorientation axis and one methyl reorientation axis are in the plane of the page whereas the other two methyl reorientation axes go into and out of the page. In (b), the *t*-butyl reorientation axis is in the plane of the page, two methyl reorientation axes come out of the page, and the third goes into the page. The ring carbon (not shown) and the three methyl carbons are on the vertices of a tetrahedron with the central carbon at its center. Similarly, three methyl hydrogens and the central carbon are on the vertices of a tetrahedron with the methyl carbon at its center. The geometry has been slightly distorted to make viewing easier.

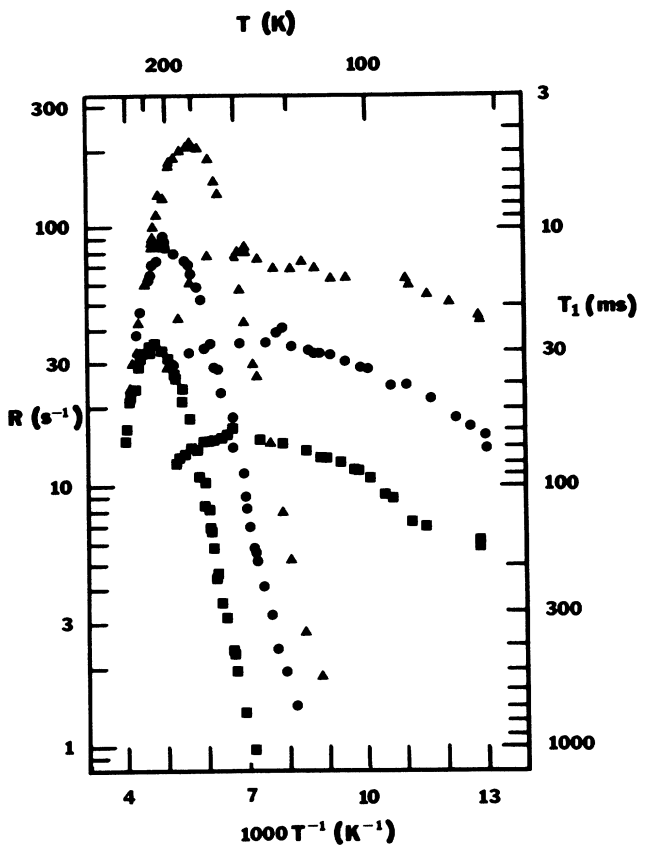

FIG. 3. $\ln(R)$ vs T^{-1} in 1,3-di-*t*-butylbenzene at 8.50 (▲), 22.5 (●), and 53.0 MHz (■). The high-temperature phase ranges from the melting point (262 K) to at least 110 K, which is the lowest temperature at which measurements were made in the high-temperature phase. It may be stable at all temperatures. The low-temperature phase ranges from 200 to at least 77 K, which is the lowest temperature at which measurements were made in the low-temperature phase. It may be stable at all temperatures below 200 K. The data in the two phases are shown separately in Figs. 4–7 and 8, respectively.

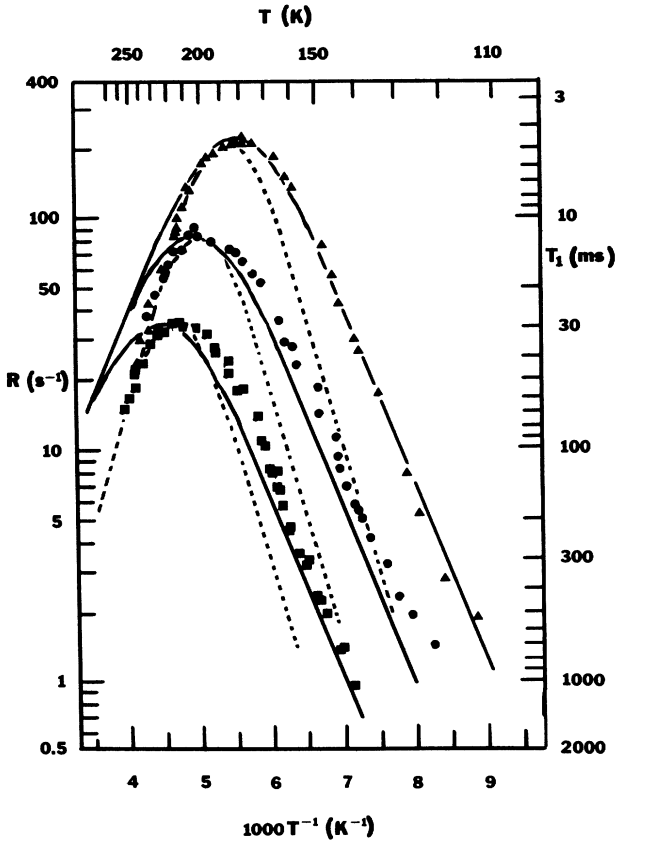

FIG. 4. $\ln(R)$ vs T^{-1} in the high-temperature phase of 1,3-di-*t*-butylbenzene at 8.50 (▲), 22.5 (●), and 53.0 MHz (■). The lines are the theoretical fits using the *A*-type *t*-butyl group model with a Bloembergen-Purcell-Pound spectral density. One set (dashed lines) fits the data at high temperatures (all frequencies) and in the vicinity of the maximum in R and the other set (solid lines) fits the data at low temperatures (8.5 MHz) and in the vicinity of the maximum in R.

II. THE NUCLEAR-SPIN RELAXATION EXPERIMENTS

The sample of 1,3-di-*t*-butylbenzene (1,3-DTB) was purchased from Aldrich Chemical. The quoted purity was 97% and the melting point was 262 K. For the NSR experiments, the room-temperature liquid sample was put in a 7-mm inside diameter sample tube, deoxygenated by bubbling dry nitrogen gas through it, frozen in liquid nitrogen, and placed in the probe.

The spin-lattice relaxation rates R (the inverses of the spin-lattice relaxation times T_1) were measured using a standard π-t-$\pi/2$-t_R pulse sequence[2,23] with the repetition period $t_R > 8.5T_1$. Three fixed-frequency Spin-Lock CPS-2 spectrometers, operating at 8.50, 22.5, and 53.0 MHz, were used in two experimental setups which differed only in their data acquisition systems. In one system, discussed elsewhere,[24] the free-induction decay was sampled with a boxcar integrator, the averaged signal was sent to a digital voltmeter, and this voltage and the accompanying time difference t (in π-t-$\pi/2$) were sent to a microcomputer for analysis. The other system employed an Analogic Data 6000 waveform analyzer with a Model 630 plug-in to receive, average, and analyze the free-induction decay. The free-induction decay was short lived; characterized by an effective spin-spin relaxation time of about 10 μs. The signal-to-noise ratio was large and the Zeeman relaxation was always exponential to within experimental error over 2 orders of magnitude in the difference magnetization. The experimental uncertainty in R was typically 5%.

Temperature was varied by means of a flow of reheated cold nitrogen gas and temperature was measured with a copper-Constantan thermocouple. Absolute temperatures are known to ± 1 K and the temperature gradient along that part of the sample inside the NMR coil varies with experimental conditions but has been determined (using two thermocouples) to always be less than 0.5 K.

The observed relaxation rates R are presented in Fig. 3, which shows both the high- and low-temperature phases.

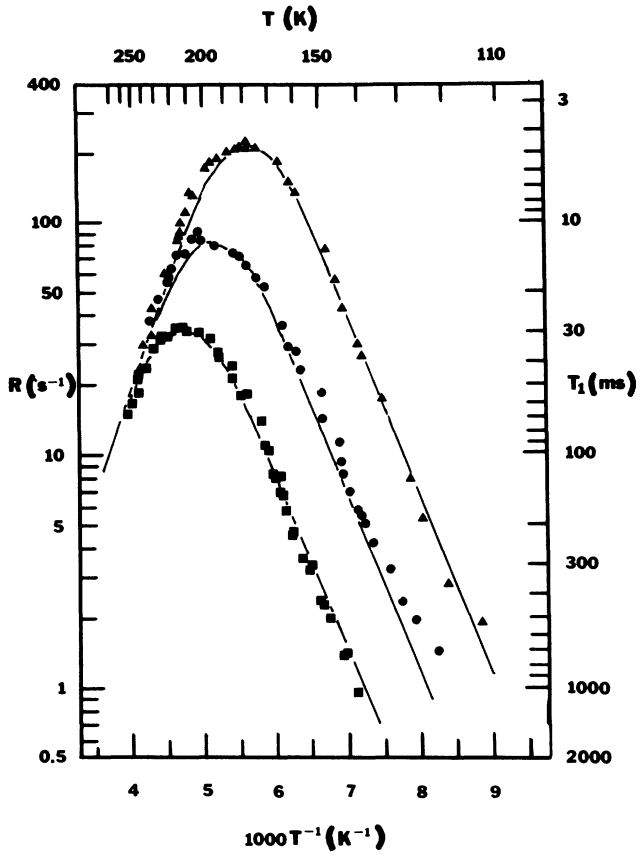

FIG. 5. $\ln(R)$ vs T^{-1} in the high-temperature phase of 1,3-di-*t*-butylbenzene at 8.50 (▲), 22.5 (●), and 53.0 MHz (■). The solid lines are the theoretical fits using the *A*-type *t*-butyl group model with a Davidson-Cole spectral density.

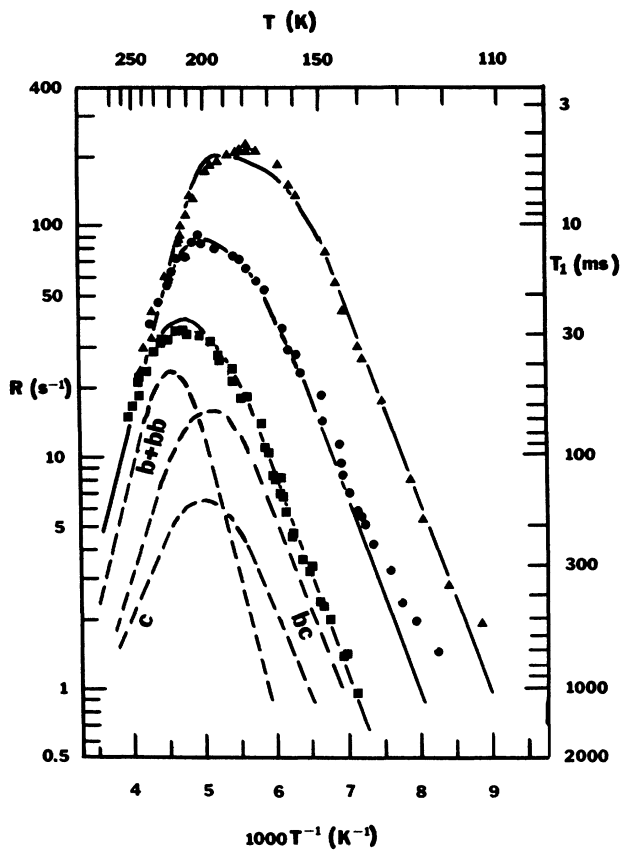

FIG. 6. $\ln(R)$ vs T^{-1} in the high-temperature phase of 1,3-di-*t*-butylbenzene at 8.50 ▲), 22.5 (●), and 53.0 MHz (■). The solid lines are the theoretical fits using the *B*-type *t*-butyl group model with a Bloembergen-Purcell-Pound spectral density. The 8.5-MHz data at high and low temperatures were used to generate the fit and the various contributions in Eq. (17) to the relaxation at 53 MHz are identified by dashed lines.

The high-temperature phase data and the low-temperature phase data are shown separately in Figs. 4–7 and Fig. 8, respectively. We are not equipped to do extremely accurate thermometry or calorimetry but we strove for preparation consistency. After degassing, the sample was always frozen in liquid nitrogen and placed in the probe which was at a preset temperature. Each determination of R took about 15 min and at least 15 min was allowed for the sample to come to equilibrium after a temperature change. On cooling from just below the melting point of 262 K, it was found that the sample was always in the high-temperature phase and remained in the high-temperature phase down to 110 K, which was the lowest temperature at which R values were measured in the high-temperature phase. Based on the theoretical fits discussed below, it is most likely that the high-temperature phase is the crystalline structure. It is probably stable to below 77 K so long as the temperature is reduced slowly. When starting at 77 K, the sample was always in the low-temperature phase. On increasing temperature slowly from 77 K in the low-temperature phase, the transition from the low-temperature phase to the high-temperature phase always occurred within a few degrees of 200 K. We made some measurements while the sample was either in some "in between" state or, more likely, a mixture of the two phases and we report these measurements as low-temperature phase measurements in Fig. 8. The result is that some of the highest-temperature R values in the low-temperature phase may not be representative of that phase. They may be indicative of critical processes near the onset of a phase transition. On the basis of the analysis discussed below, we suggest that the low-temperature phase is probably a phase with no long-range structural order.

III. THEORY

A. General dipole-dipole relaxation theory

For the molecular solids of interest, the proton Zeeman relaxation results from the modulation of the nuclear-spin dipole-dipole interactions by the intramolecular motion. For a system of spin-$\frac{1}{2}$ pairs in contact with a heat bath characterized by a temperature T and a magnetic field strength $B=\omega/\gamma$, the observed Zeeman relaxation rate R is of the form

$$R(\omega,T)=Ah(\omega,T)\ . \tag{1}$$

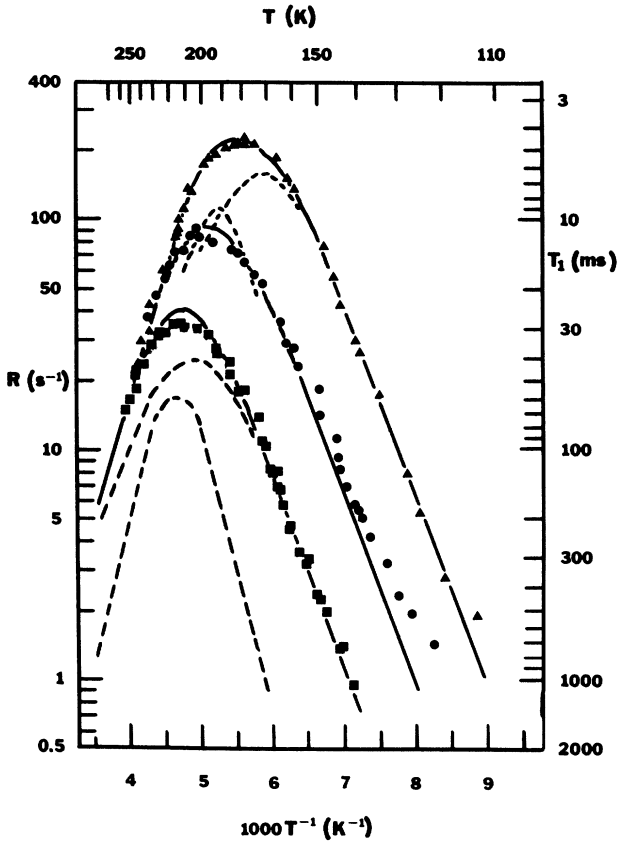

FIG. 7. $\ln(R)$ vs T^{-1} in the high-temperature phase of 1,3-di-*t*-butylbenzene at 8.50 (▲), 22.5 (●), and 53.0 MHz (■). The solid lines are the theoretical fits using the *A*-type *t*-butyl group two-site model. Bloembergen-Purcell-Pound spectral densities are used and the two components are shown for 53 MHz and in the vicinity of the maximum in R at 8.50 MHz. The 8.5-MHz data at high and low temperatures were used to generate the fit.

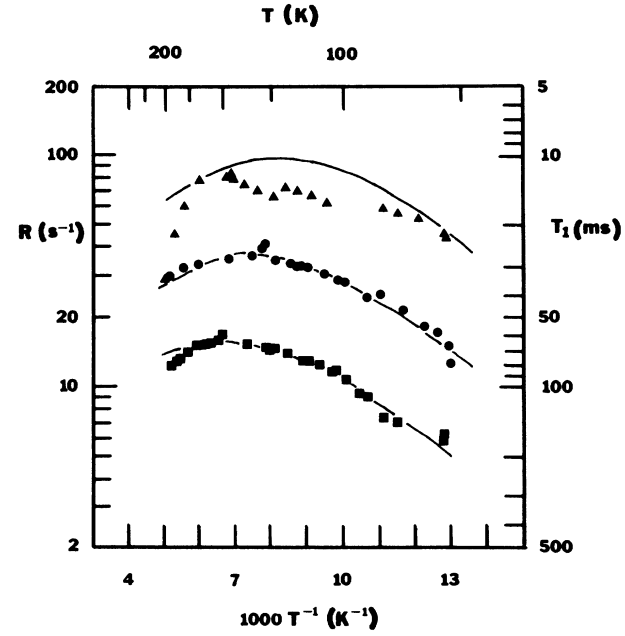

FIG. 8. $\ln(R)$ vs T^{-1} in the low-temperature phase of 1,3-di-*t*-butylbenzene at 8.50 (▲), 22.5 (●), and 53.0 MHz (■). The solid lines are the theoretical fits using the single *A*-type *t*-butyl group model with a Havriliak-Negami spectral density.

A physical interpretation of Eq. (1) is obtained from Fermi's Golden Rule No. 2.[25,26] The parameter A is a measure of the strength of the dipole-dipole interaction and is determined by the geometry and the number of interacting protons. The parameter h is a sum over spectral densities and depends on the nuclear Larmor angular frequency ω and on a series of parameters $x_1,x_2,x_3,\ldots$ which characterize the reorientation process. Relating the thermodynamic observables such as temperature T (or pressure P[10]) to the microscopic parameters is one of the main goals of the research. $h(\omega,x_1,x_2,x_3,\ldots)$ is written in terms of the spectral density $j(\omega,x_1,x_2,x_3,\ldots)$:[1,2]

$$h(\omega,x_1,x_2,x_3,\ldots)=j(\omega,x_1,x_2,x_3,\ldots)+4j(2\omega,x_1,x_2,x_3,\ldots)\ , \quad (2)$$

where the two terms have their origin in the fact that those parts of the pairwise dipole-dipole interaction involved with Zeeman relaxation correspond to both single and double spin flips.

The spectral density is the Fourier transform of the correlation function $g(t)$:

$$j(\omega,x_1,x_2,x_3,\ldots)=\int_{-\infty}^{\infty} g(t,x_1,x_2,x_3,\ldots)e^{i\omega t}dt\ , \quad (3)$$

with the normalization

$$\int_0^{\infty} j(\omega,x_1,x_2,x_3,\ldots)d\omega=\pi\ . \quad (4)$$

B. Systems with *t*-butyl groups

The dipole-dipole interaction energy for two spins is proportional to r^{-3} (where r is the spin separation) so the factor A in Eq. (1) is proportional to r^{-6}. For Zeeman relaxation in molecular solids where the only motion is methyl reorientation, one need only consider couplings between protons in methyl groups and between methyl protons and other protons. Other proton-proton vectors are not being modulated by the motion. For a methyl group, the three protons are $r=0.18$ nm apart which, on average, is much smaller than the distances between a methyl proton and other protons. Thus, in systems where methyl groups are relatively isolated, considering only the intramethyl contribution to the total relaxation rate is often an excellent approximation.[9] The relaxation for this fixed triangle or protons and closely related systems has been discussed very thoroughly for many years[27–30] but the form of the spectral density $j(\omega,x_1,x_2,x_3,\ldots)$ for all but a few simple systems remains an unsolved problem.

In general, for three or more coupled spin-$\frac{1}{2}$ particles, a perturbed nuclear magnetization will not relax exponentially, but rather via a sum of exponentials.[1] For a methyl group, there is the added complication that the motions of the three proton-proton vectors are completely correlated and this gives rise to cross correlations (which also result in nonexponential relaxation) as well as autocorrelations.[31–33] Indeed, nonexponential relaxation

is sometimes observed in systems where only methyl reorientation is occurring.[34,35]

For a t-butyl group, the methyl reorientation is superimposed on t-butyl reorientation as shown in Fig. 2. This often simplifies the description of the dynamics because the superimposed reorientations make the motion of each proton-proton vector less restricted (i.e., they are not reorienting in only a single plane) and this tends to destroy the effects of cross correlations.[33] Thus nonexponential relaxation due to cross-correlation effects is usually not observed in systems where t-butyl groups are reorientating[17,20,24,36,37] and theoretical expressions for the single relaxation rate can be obtained in straightforward ways since only autocorrelation functions need be considered. This allows for more stringent testing of the assumptions concerning which dipole-dipole interactions need to be taken into account. This also allows for more stringent testing of models for the form of the spectral density.

The relaxation rate in molecular solids where superimposed methyl and t-butyl group reorientation is occurring has been discussed[18] and we review it here. The total observed relaxation rate is

$$R=\sum_{i=1}^{M}\left[\frac{9}{N}R_i^{\text{inter}}+\sum_{j=1}^{3}\frac{3}{N}R_{ij}^{\text{intra}}\right], \tag{5}$$

where R_{ij}^{intra} is the relaxation rate due to the dipole-dipole interactions between the three protons in the jth methyl group which, in turn, is in the ith t-butyl group. The index j runs over the three methyl groups in the ith t-butyl group. R_i^{inter} takes into account the intermethyl, intra-t-butyl interactions for the ith t-butyl group. There are M ($=2$ for DTB) t-butyl groups in the molecule. The dipole-dipole interactions between the nine protons in a t-butyl group and other protons is not considered. Not only is r^{-6} usually very small for these terms but the modulation of the orientation of $\mathbf{r}$ with respect to the field is considerably less than for intra-t-butyl $\mathbf{r}$ vectors, all of which reorient through 360° in at least one plane. In Eq. (5), n/N is the ratio of the number of protons in the mobile unit (methyl or t-butyl) to the total number of protons in the molecule. ($n=3$ for a methyl group, $n=9$ for a t-butyl group, and $N=22$ for DTB.) This assumes that spin diffusion is rapid, which means that mutual spin flips transmit changes in local proton magnetization throughout all hydrogen protons in the molecular and the solid on a time scale $T_2\sim 10$ μs, which is orders of magnitude faster than $T_1=R^{-1}>5$ ms. Thus the relaxation process is slowed down as the "relaxing" protons relax the "nonrelaxing" protons and R is decreased by n/N.[38]

Crudely, the correlation time τ is the mean time between changes in the local field, which is the same as the mean time between methyl or t-butyl group hops between equivalent positions. In the simplest case, the correlation time can be defined rigorously as the area under the correlation function $g(t)$ in Eq. (3):

$$\tau=\tfrac{1}{2}j(0)=\tfrac{1}{2}\int_{-\infty}^{\infty}g(t)dt\ . \tag{6}$$

This definition is not suitable for more complicated forms of j as discussed in Sec. III D. τ is further parametrized in terms of more fundamental parameters which characterize the anisotropic electrostatic potentials.

If the reorientation of the jth methyl group in the ith t-butyl group is characterized by the correlation time τ_{ij} and the reorientation of the ith t-butyl group itself is characterized by τ_i, R_{ij}^{intra} is given by[39,40]

$$\begin{aligned}R_{ij}^{\text{intra}}=\tfrac{3}{10}A^{\text{intra}}[&\tfrac{2}{9}h(\omega,\tau_{ij},x_2,x_3,\ldots)\\&+\tfrac{2}{9}h(\omega,\tau_i,x_2,x_3,\ldots)\\&+\tfrac{19}{36}h(\omega,\tau_{i,ij},x_2,x_3,\ldots)]\end{aligned} \tag{7}$$

where the dipole-dipole strength parameter is

$$A^{\text{intra}}=\left[\frac{\mu_0}{4\pi}\right]^2\frac{\gamma^4\hbar^2}{r^6}\ . \tag{8}$$

The proton-proton separation in a methyl group is $r=1.797\times10^{-10}$ m, $\mu_0/(4\pi)=10^{-7}$ m kg s^{-2} A^{-2} where μ_0 is the permeability of free space, the proton magnetogyric ratio is $\gamma=2.675\times10^{8}$ kg^{-1} s A, and $\hbar=1.054\times10^{-34}$ m^2 kg s^{-1}. The numerical value of A^{intra} is 1.69×10^{10} s^{-2}. The first and second terms in Eq. (7) result from the reorientation of the methyl and t-butyl groups, respectively, and the third term results from the superposition of the two motions. The correlation time $\tau_{i,ij}$ in this third term is defined by

$$\tau_{i,ij}^{-1}=\tau_i^{-1}+\tau_{ij}^{-1} \tag{9}$$

and can be associated with the superposition of the two motions. The proton-proton separation r contained in Eq. (8) does not change with time and the spectral density involves only the dynamics of the spherical angles of $\mathbf{r}$.

If $\tau_i=\infty$ in Eq. (7) (i.e., no t-butyl reorientation) then the second term vanishes [since $h(\omega,\tau_i)$ must approach 0 as $\tau_i\to0$ or ∞], and $\tau_{i,ij}=\tau_{ij}$, which can be seen from Eq. (9). In this case, the first and third terms of Eq. (7) can be added, $\frac{2}{9}+\frac{19}{36}=\frac{3}{4}$, and one obtains the standard expression for the relaxation due to a reorienting methyl group:[29,39]

$$R_{ij}^{\text{intra}}=\tfrac{3}{10}A^{\text{intra}}[\tfrac{3}{4}h(\omega,\tau_{ij},x_2,x_3,\ldots)]\ . \tag{10}$$

Because the distances between the protons on different methyl groups in the same t-butyl group change as the methyl groups reorient, a closed form expression for R^{inter} is cumbersome. An approximate expression can be obtained by condensing the three protons of each methyl group to the center of the methyl triangle and considering the interaction between these three systems. This is an excellent approximation for $\tau_{ij}\ll\tau_i$ which will be the case for the model discussed in Sec. III C 2. However, in the models discussed in Secs. III C 1 and III C 3, we will assume $\tau_{ij}=\tau_i$, in which case the accuracy of the approximation is not clear. If we make this approximation, R^{inter} is three times R^{intra} in Eq. (10) with A^{intra} replaced with A^{inter} and τ_{ij} replaced with τ_i:[41]

$$R_i^{\text{inter}}=3\tfrac{3}{10}A^{\text{inter}}[\tfrac{3}{4}h(\omega,\tau_i,x_2,x_3,\ldots)]\ , \tag{11}$$

where

$$A^{\text{inter}}=\left[\frac{\mu_0}{4\pi}\right]^2\frac{\gamma^4\hbar^2}{r_*^6}=\left[\frac{r}{r_*}\right]^6 A^{\text{intra}} \tag{12}$$

and where $r_*=3.12\times10^{-10}$ m. $A^{\text{inter}}=6.23\times10^8\ \text{s}^{-1}$.

The relative importance of the intra-*t*-butyl, intermethyl relaxation rate given by Eq. (11) can be estimated from the ratio $3A^{\text{inter}}/A^{\text{intra}}=0.11$. This means that using the approximation for R^{inter} in Eq. (11) in models which do not satisfy the conditon $\tau_{ij}\ll\tau_i$ should not lead to serious error.

The total relaxation rate is now obtained by substituting Eqs. (7) and (11) into Eq. (5). This expression is valid for a wide range of systems because it is quite general. It is also a lower limit because all methyl-nonmethyl dipole-dipole interactions have been ignored.

C. Specific relaxation models for 1,3-DTB

In order to apply the general theory to systems like DTB we must model the local electrostatic environment of the *t*-butyl groups and their constituent methyl groups. To begin with, we need only specify the symmetry of the environment. We will investigate three models. First, we consider the case where all three methyl groups are dynamically equivalent. In this case, the *t*-butyl group and the constituent methyl groups are characterized by the same correlation time. This is the situation in the 1.4 isomer.[17] Second, we consider the situation where two of the three methyl groups in the dynamically equivalent *t*-butyl groups are themselves dynamically equivalent but dynamically inequivalent to the third methyl group. Third, we investigate an extension of the first model but with two inequivalent sites. This model mimics a crystal structure which leads to two different *t*-butyl group environments. The first model is a one-τ model and the second and third are two-τ models.

1. A-type t-butyl groups: A one-τ model

The model used to fit the 1,4-DTB data[17] involves a single correlation time. Considering only single molecule symmetry, the two *t*-butyl groups in 1,4-DTB are dynamically equivalent, so that the sum over i in Eq. (5) gives two identical terms. Also, the three methyl groups are equivalent and the three terms in the sum over j are identical. This is equivalent to saying that the *t*-butyl groups reorient in sixfold potential wells. The surprising result for 1,4-DTB is that the methyl reorientation is characterized by the same correlation time as the *t*-butyl group.[17,18] In this case, the *t*-butyl groups are called *A* type and the three constituent methyl groups are called *a* type. If nearest neighbors on the ring (protons on both sides for both isomers) dominate in determining the symmetry of the reorienting group, then the 1,3 and 1,4 isomers are the same. With these assumptions, $\tau_i=\tau_{ij}\equiv\tau_a$ (for *a* type) and, using Eq. (9), $\tau_{i,ij}=(\tau_a^{-1}+\tau_a^{-1})^{-1}=\tau_a/2$. The relaxation rate in Eq. (5) becomes

$$R=\tilde{A}_a h(\omega,\tau_a,x_2,x_3,\ldots)+\tilde{A}_{aa}h(\omega,\tau_a/2,x_2,x_3,\ldots), \tag{13}$$

with

$$\tilde{A}_a=\tfrac{18}{22}\tfrac{3}{10}(3\tfrac{3}{4}A^{\text{inter}}+\tfrac{4}{9}A^{\text{intra}})=2.19\times10^9\ \text{s}^{-2} \tag{14}$$

and

$$\tilde{A}_{aa}=\tfrac{18}{22}\tfrac{3}{10}(\tfrac{19}{36}A^{\text{intra}})=2.19\times10^9\ \text{s}^{-2}. \tag{15}$$

The numerical values of $\tilde{A}_a$ and $\tilde{A}_{aa}$ are the same to within 0.5%. This is accidental since A^{intra} depends on r and A^{inter} depends on r_*. Using Eqs. (2) and (13), we write the Zeeman relaxation rate as

$$R=\tilde{A}_a[j(\omega,\tau_a,\{x_k\})+4j(2\omega,\tau_a,\{x_k\})+j(\omega,\tau_a/2,\{x_k\})+4j(2\omega,\tau_a/2,\{x_k\})], \tag{16}$$

where we have used the fact that $\tilde{A}_{aa}=\tilde{A}_a$.

2. B-type t-butyl groups: A two-τ model

In the second model, the two *t*-butyl groups are equivalent and are called *B* types.[18,24,36] They reorient in a threefold potential rather than in a sixfold potential. In each *t*-butyl group, two of the three methyl groups (called *c* types) are dynamically equivalent, one being above and the other being below the plane of the ring. The third methyl group (called a *b* type) is in the plane of the ring close to a ring proton. The geometry can be visualized with the help of Fig. 2. In this model, the reorientation of the *c*-type methyl group is characterized by a correlation time τ_c and the reorientation of the *B*-type *t*-butyl group and its constituent *b*-type methyl group is characterized by a correlation time τ_b. The *b*-type methyl group and the *B*-type *t*-butyl group have the same correlation time associated with their dynamics. For this second model, the two terms in the sum over i in Eq. (5) are identical but there are two different terms in the sum over j, one for the *b* process and one for the *c* process. Equation (5) then becomes

$$R=\tilde{A}_b h(\omega,\tau_b,x_2,x_3,\ldots)+\tilde{A}_{bb}h(\omega,\tau_b/2,x_2,x_3,\ldots)+\tilde{A}_c h(\omega,\tau_c,x_2,x_3,\ldots)+\tilde{A}_{bc}h(\omega,\tau_{bc},x_2,x_3,\ldots) \tag{17}$$

with $\tau_{bb}=(\tau_b^{-1}+\tau_b^{-1})^{-1}=\tau_b/2$ and $\tau_{bc}=(\tau_b^{-1}+\tau_c^{-1})^{-1}$ using Eq. (9). Equation (17) for this two-τ model can be compared with Eq. (13) for the one-τ model. The four multipliers in Eq. (17), along with their numerical values, are given by

$$\tilde{A}_b=\tfrac{3}{10}(\tfrac{18}{22}3\tfrac{3}{4}A^{\text{inter}}+\tfrac{6}{22}\tfrac{8}{9}A^{\text{intra}})=1.57\times10^9\ \text{s}^{-2}, \tag{18}$$

$$\tilde{A}_{bb}=\tfrac{6}{22}\tfrac{3}{10}(\tfrac{19}{36}A^{\text{intra}})=7.29\times10^8\ \text{s}^{-2}, \tag{19}$$

$$\tilde{A}_c=\tfrac{12}{22}\tfrac{3}{10}(\tfrac{2}{9}A^{\text{intra}})=6.14\times10^8\ \text{s}^{-2}, \tag{20}$$

and

$$\tilde{A}_{bc}=\tfrac{12}{22}\tfrac{3}{10}(\tfrac{19}{36}A^{\text{intra}})=1.45\times10^9\ \text{s}^{-2}. \tag{21}$$

The relaxation rate [analagous to Eq. (16) for the one-τ model] is now obtained from Eqs. (2) and (17). The result

has the form of Eq. (16) but there are now eight terms involving the four correlation times τ_b, $\tau_{bb}=\tau_b/2$, τ_c, and τ_{bc} and the four multipliers in Eqs. (18)–(21).

3. *Inequivalent sites: A two-τ model*

In the third model, R is given by the sum of two terms like Eq. (16), each with its unique τ value, because the crystal structure leads to inequivalent t-butyl group sites:

$$R=\sum_{i=1}^{2}\tilde{A}_a^{(i)}[j(\omega,\tau_a^{(i)},\{x_k\})+4j(2\omega,\tau_a^{(i)},\{x_k\}) +j(\omega,\tau_a^{(i)}/2,\{x_k\})+4j(2\omega,\tau_a^{(i)}/2,\{x_k\})] \tag{22}$$

where the theoretical values of the $\tilde{A}_a^{(i)}$ depend on the crystal structure. Their sum must add up to $\tilde{A}_a$ in Eq. (14).

Another approach to the general problem is to assume a continuous distribution of τ values. This is best done via the form of the spectral density.

D. The spectral density

1. *The Bloembergen-Purcell-Pound spectral density*

If the motion is random and all molecules are in identical environments, the correlation function is a simple exponential,

$$g(t)=e^{-|t|/\tau} . \tag{23}$$

Using Eq. (3), the spectral density is[1,2]

$$j(\omega,\tau)=\frac{2\tau}{1+\omega^2\tau^2} . \tag{24}$$

This is the Bloembergen-Purcell-Pound (BPP) spectral density.[42]

2. *Distributions of correlation times*

There are two quite different physical reasons why the spectral density appropriate for Poisson statistics [Eq. (24)] might not apply. One is that there may be subgroups of inequivalent groups of rotors. Although each subgroup has its dynamics described by Poisson statistics, each subgroup has a different mean frequency τ^{-1}. This will be the case in a glass where there are many different environments for methyl groups[43] but this can also be the case for crystalline solids such as 2,3-dimethylanthracene and 2,3-dimethylnaphthalene where the form of the crystal structure leads to a large variety of local environments.[44] In this case, a general spectral density can be formed from a distribution of BPP spectral densities, each characterized by a correlation time ξ. The spectral density becomes

$$j(\omega,x_1,x_2,\ldots)=\int_0^\infty \Lambda(\xi,x_1,x_2,\ldots)\frac{2\xi}{1+\omega^2\xi^2}d\xi , \tag{25}$$

where the distribution function Λ is normalized,

$$\int_0^\infty \Lambda(\xi,x_1,x_2,\ldots)d\xi=1 . \tag{26}$$

There is a question as to when one should assume a continuous distribution of τ values and when one should use a finite number of BPP spectral densities, each with its unique τ value. We shall address this question in Sec. IV.

Another approach is to assume that the correlation function is not a simple exponential. Although perhaps physically quite different, the two approaches can be made formally identical since the Fourier transform in Eq. (3) and its inverse,

$$g(t,x_1,x_2,\ldots)=\frac{1}{2\pi}\int_{-\infty}^{\infty} j(\omega,x_1,x_2,\ldots)e^{-i\omega t}d\omega , \tag{27}$$

are linear operations. Thus a nonexponential correlation function can be expressed as a distribution of exponential correlation functions. Equation (25) in Eq. (27) yields

$$g(t,x_1,x_2,\ldots)=\int_0^\infty \Lambda(\xi,x_1,x_2,\ldots)e^{-t/\xi}d\xi . \tag{28}$$

3. *The Havriliak-Negami spectral density*

Many non-BPP spectral densities have their origin in dielectric relaxation (DR) experiments. DR and NSR experiments are very different in that in the former, the modulation of an electric dipole vector is observed directly, whereas in the latter the *effect* of the modulation of a nucleus-nucleus vector on the nuclear- (magnetic) spin state is observed. However, the statistics that describe the dynamics can certainly be related. With the normalization adopted for $j(\omega)$, the NSR spectral density is $2/\omega$ times the imaginary part of the DR spectral density $H(\omega)$. For example, if the motion is describable by Poisson statistics, a Debye DR spectral density $H(\omega)$ is given by[45] $H(\omega)=(1+i\omega\tau)^{-1}$ and the $j(\omega)$ for the NSR case is given by Eq. (24).

Dissado and Hill (DH) have developed a very general DR spectral density[46,47] which successfully interprets many sets of DR data.[48] It has also been used to interpret mechanical relaxation data.[49] The dynamical model[45–47,50] on which this DH spectral density is based assumes both distributions of motional barriers and the presence of correlated motions. There is an asymmetric anisotropic potential and the many-body problem is introduced via a distribution of well depths. This distribution is characterized by a parameter n where $0<n<1$. The value of n depends on the details of the averaging procedure and is material dependent. A value of $n=0$ corresponds to a unique barrier height and a value of $n=1$ corresponds to the greatest allowed distribution of barrier heights. Correlated motions among the dipoles will affect the relaxation and this is characterized by a parameter m, $0<m<1$ where $m=1$ corresponds to no correlated motions and $m=0$ corresponds to perfectly correlated motions.

The DH spectral density $H(\omega)$ for this model[46,47] requires numerical evaluation of confluent hypergeometric functions. We find it preferable to deal with simpler algebraic functions if possible and we note, as previously pointed out,[51] that the phenomenological spectral density

due to Havriliak and Negami[52] (HN) has many properties in common with the DH spectral density although it is different in appreciable ways.[53] For our purposes the HN spectral density is both sufficient and informative.

The HN spectral density for DR studies is given by $H(\omega)=[1+(i\omega\tau)^{\delta}]^{-\epsilon}$ where $0<\delta<1$ and $\epsilon<\delta^{-1}$. Although there is no fundamental theoretical relationship between the microscopic fundamental parameter pair m,n in the DH model and the phenomenological parameter pair δ,ϵ in the HN model, they can be related by fitting the same DR or NSR data. The relationship is $m=\delta$ and $n=1-\delta\epsilon$. Thus δ is a measure of the correlations and the product $\delta\epsilon$ is a measure of a spread in barriers.

The NSR spectral density corresponding to $2/\omega$ times the imaginary part of the HN DR spectral density is

$$j(\omega,\tau,\epsilon,\delta)=\frac{2\sin\left[\epsilon\arctan\left[\dfrac{(\omega\tau)^{\delta}\sin(\delta\pi/2)}{1+(\omega\tau)^{\delta}\cos(\delta\pi/2)}\right]\right]}{\omega[1+2(\omega\tau)^{\delta}\cos(\delta\pi/2)+(\omega\tau)^{2\delta}]^{\epsilon/2}} . \tag{29}$$

At high temperatures where τ is sufficiently small that $\omega\tau\ll 1$, j reduces to

$$j(\omega,\tau,\epsilon,\delta)=2\epsilon[\sin(\delta\pi/2)]\tau^{\delta}\omega^{-(1-\delta)} \tag{30}$$

and, at low temperatures where $\omega\tau\gg 1$,

$$j(\omega,\tau,\epsilon,\delta)=2[\sin(\epsilon\delta\pi/2)]\tau^{-\delta\epsilon}\omega^{-(1+\delta\epsilon)} . \tag{31}$$

4. The Davidson-Cole spectral density

If $\delta=1$, the HN spectral density in Eq. (29) reduces to the Davidson-Cole (DC) spectral density[54] given by

$$j(\omega,\tau,\epsilon)=\frac{2}{\omega}\frac{\sin[\epsilon\arctan(\omega\tau)]}{(1+\omega^2\tau^2)^{\epsilon/2}} . \tag{32}$$

The DC spectral density is an important subset of the HN (or DH) spectral density because it implies that $m=1$ and there are no correlated motions. This is the usual case for NSR experiments. In terms of the NSR data, it is usually successful when $R(\omega,T)$ data is independent of ω at high temperatures ($\omega\tau\ll 1$) as in Fig. 5. Relating the remaining parameter ϵ to the DH theory, $\epsilon=1-n$ so ϵ becomes a measure of the distribution of barriers.

The DC spectral density can be obtained directly from the assumption of a distribution of BPP spectral densities via Eq. (25) with a distribution $\Lambda(\xi,\tau,\epsilon)$ given by

$$\Lambda(\xi,\tau,\epsilon)=\begin{cases}\sin(\epsilon\pi)\dfrac{1}{\pi\xi}\left[\dfrac{\xi}{\tau-\xi}\right]^{\epsilon}, & \xi<\tau\\ 0, & \xi>\tau .\end{cases} \tag{33}$$

This distribution of correlation times seems not very physical since there are singularities at $\xi=0$ and $\xi=\tau$ but a meaningful distribution of activation energies can be derived from it as discussed in Sec. IV D. The fact that $\Lambda(\xi)\propto\xi^{-(1-\epsilon)}$ (with $0<\epsilon<1$) as $\xi\to 0$ is not physically meaningful since ξ will not go to zero but rather to some ξ_0. Again, this is discussed in Sec. IV. The singularity at $\xi=\tau$ corresponds to the unique BPP correlation time since Λ in Eq. (33) approaches $\delta(\tau-\xi)$ (where δ is a Dirac δ function) as $\epsilon\to 1$ and j in Eq. (32) approaches j in Eq. (24).

For completeness, we note that if $\epsilon=1$, the HN spectral density in Eq. (29) reduces to the Cole-Cole spectral density which has been used extensively in DR studies.[51]

E. The correlation time

There remains the relationship between the correlation time τ and the temperature T. This matter is discussed in Ref. 9, where several models are given. The experiments discussed here are performed in the high-temperature "classical hopping" regime where the details of the phonon spectrum that make up the lattice do not matter. The phonons make up an infinite heat capacity thermal reservoir that is characterized by the bulk equilibrium temperature. The energies of the nuclear-spin reservoir are completely negligible. The transition from the low-temperature tunneling regime, which may be sensitive to the structure of the phonon spectrum, to this high-temperature classical hopping regime is of considerable interest and is being studied intensively.[55–57]

The simplest model for τ is to assume an Arrhenius relationship,

$$\tau=\tau_{\infty}e^{E/kT} , \tag{34}$$

where E is an effective activation energy which is either equal or nearly equal to the barrier height for $E\gg kT$ (Ref. 58) and where the parameter τ_{∞} is discussed below. Equation (34) ties together the two approaches to non-BPP NSR data in that the distribution of correlation times leads directly to a distribution of effective activation energies which is inherent in the DH model for DR relaxation.

A physical interpretation of the parameter τ_{∞} in Eq. (34) can be obtained by assuming that there is a simple periodic potential of height $E\gg kT$ and that reorientation occurs by thermally activated rotation over the top of the barrier as discussed above. The reorientation rate τ^{-1} in Eq. (34) is the product of the probability of being near the top of the well, $\exp(-E/kT)$, and the attempt frequency, τ_{∞}^{-1} (i.e., the frequency the rotor has when it does happen to be near the top of the well). In the harmonic approximation, this attempt frequency may be approximated by the vibrational frequency. We call this frequency $\bar{\tau}_{\infty}^{-1}$ and $\bar{\tau}_{\infty}$ is given by[59]

$$\bar{\tau}_{\infty}=\left[\frac{2\pi}{3}\right]\left[\frac{2I}{E}\right]^{1/2} \tag{35}$$

where I is the moment of inertia for the reorienting group. For a methyl group, $I=5.3\times10^{-47}$ kg m^2 and for a t-butyl group, I is approximately 2.4×10^{-45} kg m^2.

IV. DATA ANALYSIS AND DISCUSSION

A. Parametrization of the data

The observed $R(\omega,T)$ for 1,3-DTB are shown in Fig. 3. The high- and low-temperature phases are shown separately in Figs. 4–7 and 8, respectively. In both 1,4-DTB (Ref. 17) and the high-temperature phase of 1,3-DTB (Figs. 4–7), $\ln(R)$ versus T^{-1} is linear at both high and low temperatures. A convenient parametrization of the data in this case is to fit the slopes and intercepts in these regions. This parametrization is independent of any theoretical considerations. At high temperatures,

$$\ln(R)=\mathcal{A}T^{-1}+\mathcal{B} \tag{36}$$

and at low temperatures,

$$\ln(R)=-\mathcal{C}T^{-1}+\mathcal{D} \tag{37}$$

where $\mathcal{A}$, $\mathcal{B}$, $\mathcal{C}$, and $\mathcal{D}$ are positive constants. (The slope at low temperatures is $-\mathcal{C}$, which is negative for $\mathcal{C}>0$.)

Below, we present a single one-τ fit of the low-temperature data using the HN spectral density. This procedure will assume that the t-butyl group is A type as discussed in Sec. III C 1. For the high-temperature data, we will employ a variety of one-τ and two-τ models.

We first relate, within the confines of a one-τ model, the parameters characterizing the HN spectral density and those characterizing the experimental data. The DC and BPP spectral densities are then treated as limiting cases of the HN spectral density. If we assume that the t-butyl group is A type and if we use the HN spectral density, R is given by Eqs. (16), (29), and (34) and there are five fitting parameters, A_a, E_a, $\tau_{a\infty}$, δ, and ϵ. There are theoretical values for A_a and $\tau_{a\infty}$ (called $\tilde{A}_a$ and $\tilde{\tau}_{a\infty}$) given by Eqs. (14) and (35) with which the experimentally determined values can be compared. This set of five parameters is related to the experimental parameter set $\mathcal{A}$, $\mathcal{B}$, $\mathcal{C}$, and $\mathcal{D}$ in Eqs. (36) and (37) by

$$\mathcal{A}=\frac{\delta E_a}{k}\ , \tag{38}$$

$$\mathcal{B}=\ln\left[2(3+2^{1+\delta}+2^{-\delta})\epsilon A_a\sin\left[\frac{\delta\pi}{2}\right]\tau_{a\infty}^{\delta}\omega^{-1+\delta}\right]\ , \tag{39}$$

$$\mathcal{C}=\frac{\delta\epsilon E_a}{k}\ , \tag{40}$$

and

$$\mathcal{D}=\ln\left[2(3+2^{1-\delta\epsilon}+2^{\delta\epsilon})\times A_a\sin\left[\frac{\delta\epsilon\pi}{2}\right]\tau_{a\infty}^{-\delta\epsilon}\omega^{-1-\delta\epsilon}\right]\ . \tag{41}$$

The two slopes [Eqs. (38) and (40)] are independent of ω, whereas the two intercepts [Eqs. (39) and (41)] do depend on ω so that measurements at high and low temperatures at two frequencies overdetermines the parameters.

If a two-τ model is used, the data analysis is somewhat more complicated. Using the HN spectral density with a two-τ model leads to ten parameters, which is unecessarily large. When the HN and DC spectral densities are used with a one-τ model (five and four parameters, respectively) they are mimicking a multi-τ model using the BPP spectral density. Two-τ models should be used only with BPP spectral densities unless the two τ values are so different as to lead to clearly separated maxima in R.[36]

The HN spectral density in Eq. (29) reduces to the DC spectral density in Eq. (32) for $\delta=1$. For the one-τ models, it follows from setting $\delta=1$ in Eqs. (38)–(41) that the high-temperature slope, $\mathcal{A}$, gives E_a and the ratio of the high- and low-temperature slopes, $\mathcal{C}/\mathcal{A}$, gives ϵ. A_a and $\tau_{a\infty}$ then follow from $\mathcal{B}$ and $\mathcal{D}$ in Eqs. (39) and (41). $\mathcal{B}$ is independent of ω (for $\delta=1$) whereas $\mathcal{D}$ is proportional to $\omega^{-(1+\epsilon)}$. Thus the parameter ϵ determines not only the ratio of the low- to high-temperature slopes for fixed ω but it also determines the ratios $R(\omega_1)/R(\omega_2)$ for $\omega\tau\gg1$ (low temperature). This is a very restrictive requirement. The fitting procedure for the DC spectral density is discussed elsewhere.[9] Measuring at three frequencies far overdetermines the parameters; if one obtains $\mathcal{A}$, $\mathcal{B}$, $\mathcal{C}$, and $\mathcal{D}$ at one frequency then the fits at other frequencies are completely determined with no adjustable parameters.

The BPP spectral density follows from the DC spectral density by setting $\epsilon=1$. Again, within the confines of one-τ models, it follows from Eqs. (38)–(41) that $\mathcal{A}=\mathcal{C}=\mathcal{E}_a/k$, $\mathcal{B}=\ln(15A_a\tau_{a\infty})$, and $\mathcal{D}=\ln(12A_a\tau_{a\infty}^{-1}\omega^{-1})$. Thus $R\propto\omega^{-1}$ at low temperatures ($\omega\tau_a\gg1$).

The Larmor-frequency dependence of R places a considerable constraint on the form of the spectral density and can be used to determine whether or not the observation of $\mathcal{A}\neq\mathcal{C}$ can be built up from a sum of BPP spectral densities each with a unique τ.

B. Data analysis: The high-temperature phase

1. The one-τ model

The high-temperature linear $\ln(R)$ versus T^{-1} in Figs. 4–7 is independent of ω. If we begin with a one-τ model and assume that the relaxation is given by Eq. (16), then $\delta=1$. On the other hand, $\mathcal{A}$ and $\mathcal{C}$ are different so the BPP spectral density will not work but it is instructive to show this in order to point out that the observed value of $\mathcal{A}/\mathcal{C}\sim0.9$ is significantly less than unity. In Fig. 4 we show two sets of fits using Eqs. (16), (24), and (34). In each case there are three parameters; A_a, E_a, and $\tau_{a\infty}$ and the two sets of fits correspond to forcing $\mathcal{A}=E_a/k$ (fit to the high-temperature slope) and then $\mathcal{C}=E_a/k$ (fit to the low-temperature slope). In both cases, the region of the maximum in R was also fitted.

In Table I, the parameters A_a and $\tau_{a\infty}$ are given in terms of the ratios $A_a/\tilde{A}_a$ and $\tau_{a\infty}/\tilde{\tau}_{a\infty}$ where $\tilde{A}_a$ is the theoretical value given by Eq. (14) and $\tilde{\tau}_{a\infty}$ is given by Eq. (35) with $E=E_a$. We have used the moment of inertia of the methyl group. Since $\tilde{\tau}_\infty\propto I^{1/2}$, $\tilde{\tau}_{a\infty}(t\text{-butyl})/\tilde{\tau}_{a\infty}(\text{methyl})\sim6.8$, which means the ratios $\tau_{a\infty}/\tilde{\tau}_{a\infty}$ in Table I should be divided by 6.8 if $\tilde{\tau}_{a\infty}$ for a

TABLE I. Relaxation rate parameters for one-τ models.

Molecule	Phase	$j(\omega)$	Figure reference	Fit	E_a (kJ/mol)	$A_a/\tilde{A}_a$	δ	ϵ	$\tau_{a\infty}/\tilde{\tau}_{a\infty}$
1,4-DTB		DC	Ref. 16	Good	18±1	1.17±0.06	1	0.89±0.09	0.60±0.06
1,3-DTB	High T	BPP	Fig. 4	Poor	20±1	1.00±0.05	1	1	0.23±0.02
1,3-DTB	High T	BPP	Fig. 4	Poor	14±1	1.00±0.05	1	1	8.3±0.8
1,3-DTB	High T	DC	Fig. 5	Good	17±1	1.04±0.05	1	0.86±0.09	1.4±0.1
1,3-DTB	Low T	HN	Fig. 8	Okay	10±3	1.6±0.6	0.43±0.14	0.6±0.1	$\sim 1-10^2$

t-butyl group is used. The fits are very poor and this exercise points out the significance of $\mathcal{A}\neq\mathcal{C}$. We note, however, that the fitted value of A_a (see Table I) is given by the theoretical value to better than 1%. Were the experiments done at only one frequency, one could invoke a phase transition (i.e., to a new value of E_a) in the vicinity of the maximum but the ω dependence of R completely rules out this interpretation.

The next step from the three-parameter fits above is a four-parameter fit that corresponds to the same one-τ model but using a DC spectral density instead of a BPP spectral density. Thus, the relaxation rate is given by Eqs. (16), (32), and (34) and the quite successful fit is shown in Fig. 5. The fit for 1,4-DTB, which is all the high-temperature phase, looks very similar to Fig. 5 and is presented elsewhere.[17] The values of E_a, ϵ, $\tau_{a\infty}$, and A_a are obtained from the observed $\mathcal{A}$, $\mathcal{B}$, $\mathcal{C}$, and $\mathcal{D}$ and are given in Table I. The values of R in the vicinity of the maximum, which play no role in the fitting procedure, are reproduced very well by the DC spectral density.

For this one-τ model using the DC spectral density, the fitted value of $A_a/\tilde{A}_a\sim 1$ [with $\tilde{A}_a$ from Eq. (14)] strongly supports the important assumption that intramolecular methyl-nonmethyl spin-spin interactions and all intermolecular spin-spin interactions involving at least one methyl proton play a minor, if not negligible, role in the relaxation process. Although intermolecular proton dipole-dipole interactions are often important for NSR in many solids, there are nine closely spaced strongly interacting protons in a t-butyl group so other proton dipole-dipole interactions play a *relatively* minor role for DTB in which 18 of the 22 protons are in t-butyl groups.

2. *Two-τ models*

The next fit assumes that the t-butyl group is a B type as discussed in Sec. III C 2. There are now two distinct correlation times τ_b and τ_c and two cross terms $\tau_{bb}=\tau_b/2$ and $\tau_{bc}=(\tau_b^{-1}+\tau_c^{-1})^{-1}$ resulting from the fact that the methyl group reorientation is superimposed on the t-butyl group reorientation. We shall use a BPP spectral density and the relaxation rate is given by Eqs. (17), (2), (24), and (34). We chose to keep the ratios of the fitted to theoretical A values constant, thus preserving one of the essential features of the model. We define α by $\alpha=A_i/\tilde{A}_i$ which is independent of $i=b$, bb, c, and bc [see Eqs. (18)–(21)] and the fitting parameters are α, E_b, E_c, $\tau_{b\infty}$, and $\tau_{c\infty}$. This is a five-parameter fit and the best example is shown in Fig. 6. The fitted parameters are $\alpha=1.25$, $E_b=27$ kJ/mol, $E_c=16$ kJ/mol, $\tau_{b\infty}/\tilde{\tau}_{b\infty}=0.011$, and $\tau_{c\infty}/\tilde{\tau}_{c\infty}=1.0$. The value of α is quite reasonable and suggests that within the confines of this model, proton dipole-dipole interactions other than the intra-t-butyl group contributions are playing a small but not insignificant role. This is reasonable if the t-butyl is a B type since there must be enough asymmetry in the environment to lead to a threefold rather than a sixfold electrostatic potential. Whether this lower symmetry has its basis in the intramolecular electrostatic interactions resulting from the *meta* positioning of the t-butyl groups [see Fig. 1(b)] or whether the molecular packing (intermolecular electrostatic interactions) are responsible cannot be determined from these experiments. We note that the fitted value for $\tau_{c\infty}$ is the same as the theoretical prediction based on the very simple model given in Sec. III E. The dynamics of a B-type t-butyl group in the vicinity of $\omega\tau_c\sim 1$ is such that the c-type methyl groups are sitting above and below the plane of the aromatic ring reorienting with a mean rate $\tau_c^{-1}\sim\omega$ while the t-butyl group and the b-type methyl group adjacent to the ring proton are reorienting at the slower mean rate $\tau_b^{-1}<\tau_c^{-1}$. Thus it is meaningful to speak of isolated methyl reorientation for the c-type methyls and the simple model for $\tilde{\tau}_{c\infty}$ is relevant. On the other hand, τ_b refers to both the b-type methyl and the B-type t-butyl. As such, the simple model is not very meaningful and the ratio $\tau_{b\infty}/\tilde{\tau}_{b\infty}$ is not very significant.

In the case of the one-τ model, the term in R that involves $\tau_a/2$ does not differ qualitatively from the term in τ_a [see Eq. 16)]. Similarly, in this case, R_{bb}, the term in R that involves $\tau_b/2$, does not differ qualitatively from R_b, the term in τ_b, and the two are lumped together as R_{b+bb} as one of the three dashed lines in Fig. 6. If $\tau_b\gg\tau_c$ then it follows from Eq. (9) that $\tau_{bc}\sim\tau_c$ and the terms in R that involve τ_c and τ_{bc} can also be lumped together. This is the case for other systems[18,36,60] and the situation has been discussed for the 2,4 and 2,5 isomers of di-t-butylhydroxybenzene.[36] In the present case, however, τ_b and τ_c are sufficiently close as to make τ_{bc} look like a distinct correlation time in the range $\tau_c<\tau_{bc}<\tau_b$. Thus the components of the relaxation rate R_c and R_{bc} are distinct. We show R_{b+bb}, R_c, and R_{bc}, the three contributions to the relaxation rate R in Fig. 6.

The final model we investigate is the two-site model. The t-butyl groups are A type but there are two distinct sets of them so this is a two-τ model. We use a BPP spectral density and the relaxation rate is given by Eqs. (22), (24), and (34) with the six fitting parameters $A_a^{(i)}$, $E_a^{(i)}$,

and $\tau_{a\infty}^{(i)}$ for $i=1$ and 2. The fit in Fig. 7 is successful but this is not a foregone conclusion simply because we have one more adjustable parameter than the previous fit. The important distinction between this case and the preceding one is that here there are two BPP-like R-versus-T^{-1} curves and in the preceding case there were three because of the R_{bc} term. For convenience, we choose theoretical values $\tilde{A}_a^{(1)}=\tilde{A}_a^{(2)}=\tilde{A}_a/2$ since this would be the case if there were an equal amount of each type of t-butyl groups. The fitted values are $A_a^{(1)}/\tilde{A}_a^{(1)}=1.0\pm0.1$, $A_a^{(2)}/\tilde{A}_a^{(2)}=1.4\pm0.1$, $E_a^{(1)}=27$ kJ/mol, $E_a^{(2)}=19$ kJ/mol, $\tau_{a\infty}^{(1)}/\bar{\tau}_{a\infty}^{(1)}=0.0086$, and $\tau_{a\infty}^{(2)}/\bar{\tau}_{a\infty}^{(2)}=2.0$. The two contributions to the total relaxation rate are shown at 8.5 and 53 MHz in Fig. 7. The fit is successful but it is difficult to analyze the fitted parameters in the absence of a crystal-structure determination. The ratio $A_a^{(2)}/A_a^{(1)}\sim\frac{3}{2}$ would suggest three type-(2) t-butyls to two type-(1) t-butyls but then both A values are about 50% too large. A fit where $A_a^{(1)}=A_a^{(2)}$ is forced has been done but the fit is completely unsuccessful. One can use more than two sites but this would involve nine or more parameters. This seems unwarranted when the other models are successful with four or five adjustable parameters.

3. *Summary*

The high-temperature relaxation rate data for 1,3-DTB is fitted quite well by three models: a one-τ model for A-type t-butyl groups whose dynamics is characterized by a Davidson-Cole spectral density; a two-τ model for B-type t-butyl groups whose dynamics is characterized by a Bloembergen-Purcell-Pound spectral density; and a two-τ, two-site model where the dynamics is again characterized by a Bloembergen-Purcell-Pound spectral density. The fitted parameters for the first two cases agree very well with theoretically predicted parameters from quite specific models whereas it is not clear how to interpret the parameters for the third case in the absence of the details of the crystal structure.

C. Data analysis: The low-temperature phase

For the low-temperature phase of 1,3-DTB, limiting linear R-versus-T^{-1} behavior at high temperature is not observed because the solid transforms to the high-temperature phase. All attempts at fitting the data with one-τ and two-τ models with the BPP and DC spectral densities failed. We use the HN spectral density with the one-τ model assuming the t-butyl groups are A type. A fit is shown in Fig. 8. The fitting parameters are $\mathcal{A}$, $\mathcal{B}$, $\mathcal{C}$, and $\mathcal{D}$ in Eqs. (36)–(41). A fifth parameters is required and the product $\delta\epsilon$ is chosen for computational convenience. The data at both 22.5 and 53.0 MHz are used for the fitting procedure, with $\mathcal{A}$, $\mathcal{B}$, $\mathcal{C}$, and $\mathcal{D}$ determined from the 22.5-MHz data and $\delta\epsilon$ determined from the ratio $R(22.5\text{ MHz})/R(53.0\text{ MHz})$ at the lowest temperatures since R is proportional to $\omega^{-(1+\delta\epsilon)}$. The 8.5-MHz data has considerable scatter and the low-temperature linear regime is less precise. The fit, based on the 22.5- and 53.0-MHz data, reproduces, qualitatively, the general features of the 8.50-MHz data but quantitatively the fit is poor. The uncertainties in the parameters in Table I are significant for this low-temperature phase.

The value of $A_a/\tilde{A}_a=1.6\pm0.6$ for the low-temperature phase suggests that intermolecular proton dipole-dipole interactions are strong. This suggests that a significant number of t-butyl groups on different molecules are very close to one another. (This could be the situation in a glass.) This, in turn, is consistent with a nonzero value of δ which suggests that the motions of groups of methyl and t-butyl groups are correlated.

D. Distributions of activation energies

We have only used non-BPP spectral densities with one-τ models. The non-BPP behavior can be interpreted in terms of a nonexponential correlation function, in which case τ (τ_a in the examples used) is a unique correlation time. On the other hand, the non-BPP behavior can also be interpreted in terms of a distribution of exponential correlation functions $\exp(-|t|/\xi)$ via Eq. (28) where the distribution $\Lambda(\xi,\tau,x_2,x_3,\ldots)$ is at least partially characterized by a correlation time τ. Thus τ can be a cutoff correlation time as in the case of the DC spectral density [see Eq. (33)] or it might be a mean correlation time in other models.

Corresponding to a distribution of correlation times ξ, there will be a distribution $\Gamma(\mathcal{E},E,x_2,x_3,\ldots)$ of activation energies $\mathcal{E}$ with the cutoff or mean activation energy E corresponding to the cutoff or mean correlation time τ. The relationship between $\Gamma(\mathcal{E},E,x_2,x_3,\ldots)$ and the distribution of correlation times $\Lambda(\xi,\tau,x_1,x_2,\ldots)$ can be defined formally via

$$\Gamma(\mathcal{E},E,x_2,x_3,\ldots)d\mathcal{E}=\Lambda(\xi,\tau,x_2,x_3,\ldots)d\xi\ , \tag{42}$$

but until the relationship between the correlation time ξ and the activation energy $\mathcal{E}$ is modeled, Γ cannot be determined. On initial inspection, it might seem reasonable to relate ξ to the activation energy $\mathcal{E}$ via

$$\xi=\xi_\infty e^{\mathcal{E}/kT}\ , \tag{43}$$

in analogy with Eq. (34) for τ, which is the cutoff or mean value of ξ. The precise nature of ξ_∞ in Eq. (43) is not known, so $d\mathcal{E}/d\xi$ cannot be determined even if $\Lambda(\xi,\tau,x_2,x_3,\ldots)$ is known. So, $\Gamma(\mathcal{E},E,\epsilon)$ in Eq. (42) cannot be determined. However, as a first step, the dependence of ξ_∞ on $\mathcal{E}$ and T can be presumed to be weak compared with the dependence of ξ on $\mathcal{E}$ and T via the exponential in Eq. (43).[9] We use the DC spectral density as an example. If it is assumed that ξ_∞ in Eq. (43) is constant and equal to the cutoff τ_∞ then Eqs. (33), (42), and (43) give

$$\Gamma(\mathcal{E},E,\epsilon)=\begin{cases}\dfrac{\sin(\epsilon\pi)}{\pi(kT)}\left[\dfrac{1}{e^{(E-\mathcal{E})/kT}-1}\right]^{\epsilon}, & \mathcal{E}<E\\ 0, & \mathcal{E}>E\ .\end{cases} \tag{44}$$

This model has two problems associated with it. The first is that since the lower limit for ξ is taken as 0 [Eq. (33)], the lower limit for $\mathcal{E}$ is $-\infty$ rather than 0. This makes

no sense but is not a serious problem in that the number of rotors with $-\infty < \mathcal{E} < 0$ is completely negligible compared with the number with $0 < \mathcal{E} < E$. This has been determined numerically. To put it another way, the distribution in Eq. (33) should really span the range $\tau_\infty < \xi < \tau$ rather than $0 < \xi < \tau$ if an Arrhenius relation like Eq. (34) is to be used but it does not really matter. The second problem is far more serious. The distribution $\Gamma(\mathcal{E}, E, \epsilon)$ in Eq. (44) is strongly temperature dependent. This seems totally unphysical and is sufficient reason for rejecting Eq. (43) for ξ with a constant ξ_∞. There are other more satisfying models but they seem to have little physical basis.

For completeness, we note that a recent incoherent neutron scattering experiment[43] in a glass has used a Fuoss-Kirkwood (FK) spectral density[61] to model a distribution of correlation times. The FK spectral density will not fit the 1,3-DTB in either phase within the confines of a one-τ model nor are we aware that it has ever successfully fit any NSR data.

V. SUMMARY

We have measured the temperature and Larmor-frequency dependence of the proton Zeeman relaxation rate in the 1,3 isomer of DTB. There is a phase transition in the vicinity of 200 K and the temperature and Larmor-frequency dependence of the Zeeman relaxation rate are very different in the two phases.

We are able to interpret the high-temperature phase data in terms of several models which differ in the number of distinct characteristic correlation times and the form of the spectral density. In turn, these different models can be interpreted in terms of the different possibilities for the symmetry of the environment of the *t*-butyl groups. If the spectral density characteristic of random motion is used then a two-correlation-time model is needed. We discussed two examples of such models. On the other hand, if a one-correlation-time model is assumed then the form of the spectral density implies a distribution of correlation times which describe methyl and *t*-butyl reorientation, or, it implies a nonexponential correlation function. The parameters which quantitatively describe the overall strength of the local proton dipole-dipole interactions fit very well with the various models and cannot be used to distinguish between them. When *both* temperature *and* Larmor frequency are varied, one can distinguish between dynamically equivalent rotors whose correlation times are distributed and a small number of dynamically inequivalent rotors each with their own correlation time.

The low-temperature phase relaxation rate data is unusual. The fit of the data implies a very considerable distribution of activation energies even though the precise relationship between correlation time and activation energy is not known. The detailed form of the spectral density used to fit the data is nearly equivalent to, if not mathematically identical to, that developed by Dissado and Hill (DH) to interpret dielectric relaxation (DR) data. In the DH model, one parameters is a measure of correlated motions of electric dipoles and another parameter is a measure of a spread in activation energies. It is not clear how to interpret these parameters for NSR experiments and when the appropriate theory is done for the NSR case, there will, no doubt, be considerable modifications to the model. In the meantime, we use the DR-NSR analogy as a phenomenological guide. If the DR theory is interpreted literally, it also implies strongly correlated motions of groups of methyl and *t*-butyl groups in the low-temperature phase and this is consistent with a proton dipole-dipole strength parameter which is 60% larger than that found in the high-temperature phase. We suggest that the low-temperature phase is most likely an amorphous, glassy state with no long-range order.[62] An x-ray study is needed but this would have to be done both above and below 200 K.

Many interesting and useful conclusions concerning the dynamics in molecular solids can be made with very simple qualitative analyses of nuclear-spin relaxation data so long as both temperature and Larmor frequency are varied and both long- and short-correlation-time regions are observed. Although important boundary conditions can be placed on detailed models for the motion, nuclear-spin relaxation rate experiments must be coupled with other spectroscopies before definitive models can be formulated.

ACKNOWLEDGMENTS

Acknowledgment is made to the Petroleum Research Fund administered by the American Chemical Society, for the partial support of this research. The authors wish to thank F. B. Mallory and C. W. Mallory for many very helpful discussions. One of us (A.I.H.) gratefully acknowledges partial support by Exxon Corporation; another (E.B.K.), by Shell Corporation. Part of this work forms part of the requirements for the M.A. degree (Bryn Mawr College, 1987) for one of us (H.Y.).

[1] A. Abragam, *The Principles of Nuclear Magnetism* (Oxford University Press, Oxford, 1961).
[2] C. P. Slichter, *Principles of Magnetic Resonance* (Springer-Verlag, Berlin, 1978).
[3] F. A. Rushworth, Magn. Reson. Rev. **7**, 57 (1981).
[4] F. A. Rushworth, Magn. Reson. Rev. **7**, 197 (1982).
[5] E. Szcześniak, Mol. Phys. **58**, 551 (1986).
[6] S. Mooibroek and R. E. Wasylishen, Can. J. Chem. **63**, 2926 (1985).
[7] P. A. Beckmann and A. Wendel, J. Chem. Phys. **73**, 3514 (1980).
[8] T. Tsang and D. B. Utton, J. Chem. Phys. **64**, 3780 (1976).
[9] K. G. Conn, P. A. Beckmann, C. W. Mallory, and F. B. Mallory, J. Chem. Phys. **87**, 20 (1987).
[10] T. Hasebe and J. H. Strange, J. Chem. Soc. Faraday Trans. 2 **81**, 735 1985).
[11] H. den Adel, H. B. Brom, D. J. Ligthelm, and R. A. Wind, Physica B + C **111B**, 171 (1981).

[12]U. Walther, D. Brinkmann, G. Chapuis, and H. Arend, Solid State Commun. **27**, 901 (1978).
[13]K. Takegoshi, F. Imashiro, T. Terao, and A. Saika, J. Chem. Phys. **80**, 1089 (1984).
[14]J. Virlet, L. Quiroga, B. Boucher, J. P. Amoureux, and M. Castelain, Mol. Phys. **48**, 1289 (1983).
[15]M. Bée, W. Longueville, J. P. Amoureux, and R. Fouret, J. Phys. (Paris) **47**, 305 (1986).
[16]W. H. Flygare, *Molecular Structure and Dynamics* (Prentice-Hall, Englewood Cliffs, New Jersey, 1979).
[17]P. A. Beckmann, F. A. Fusco, and A. E. O'Neill, J. Magn. Reson. **59**, 63 (1984).
[18]P. A. Beckmann, Chem. Phys. **63**, 359 (1981).
[19]A. I. Kitaigorodsky, *Molecular Crystals and Molecules* (Academic, New York, 1973).
[20]M. C. Aronson, P. A. Beckmann, B. J. Ross, and S. L. Tan, Chem. Phys. **63**, 349 (1981).
[21]J. Haupt and W. Müller-Warmuth, Z. Naturforsch., Teil A **23**, 208 (1968).
[22]A. M. I. Ahmed, R. G. Eades, T. A. Jones, and J. P. Llewellyn, J. Chem. Soc. Faraday Trans. 2 **68**, 1316 (1972).
[23]T. C. Farrar and E. D. Becker, *Pulse and Fourier Transform NMR* (Academic, New York, 1971).
[24]A. M. Albano, P. A. Beckmann, M. E. Carrington, E. E. Fisch, F. A. Fusco, A. E. O'Neill, and M. E. Scott, Phys. Rev. B **30**, 2334 (1984).
[25]L. I. Schiff, *Quantum Mechanics* (McGraw-Hill, New York, 1968).
[26]E. Fermi, *Nuclear Physics* (University of Chicago Press, Chicago, 1950), p. 142.
[27]D. E. Woessner, J. Chem. Phys. **36**, 1 (1962).
[28]P. S. Hubbard, Phys. Rev. **109**, 1153 (1958); **111**, 1746 (1958).
[29]E. O. Stejskal and H. S. Gutowsky, J. Chem. Phys. **28**, 388 (1958). See also the footnote on p. 973 of Ref. 39.
[30]I. Solomon, Phys. Rev. **99**, 559 (1955).
[31]L. K. Runnels, Phys. Rev. A **134**, 28 (1964).
[32]R. L. Hilt and P. S. Hubbard, Phys. Rev. A **134**, 392 (1964).
[33]J. D. Cutnell and W. Venable, J. Chem. Phys. **60**, 3795 (1974).
[34]M. Mehring and H. Raber, J. Chem. Phys. **59**, 1116 (1973).
[35]A. Kumar and C. S. Johnson, Jr., J. Chem. Phys. **60**, 137 (1974).
[36]P. A. Beckmann, A. M. Cheung, E. E. Fisch, F. A. Fusco, R. E. Herzog, and M. Narasimhan, J. Chem. Phys. **84**, 1959 (1986).
[37]M. C. Aronson, P. A. Beckmann, V. Guerra, C. M. Schwamb, and S. L. Tan, Mol. Phys. **41**, 1239 (1980).
[38]J. E. Anderson and W. P. Slichter, J. Phys. Chem. **69**, 3099 (1965).
[39]M. B. Dunn and C. A. McDowell, Mol. Phys. **24**, 969 (1972).
[40]P. A. Beckmann, Mol. Phys. **41**, 1227 (1980).
[41]S. Albert, H. S. Gutowsky, and J. A. Ripmeester, Chem. Phys. **56**, 3672 (1972).
[42]N. Bloembergen, E. M. Purcell, and R. V. Pound, Phys. Rev. **73**, 679 (1948).
[43]M. Bée, F. Foulon, J. P. Amoureux, C. Caucheteux, and C. Poinsignon, J. Phys. C **20**, 337 (1987).
[44]H. Wachtel, H. Port, and H. C. Wolf, Chem. Phys. Lett. **135**, 506 (1987).
[45]R. M. Hill and A. K. Jonscher, Contemp. Phys. **24**, 75 (1983).
[46]L. A. Dissado, and R. M. Hill, Nature (London) **279**, 685 (1979).
[47]L. A. Dissado and R. M. Hill, Philos. Mag. **41**, 625 (1980).
[48]R. M. Hill, J. Mater. Sci. **16**, 118 (1981).
[49]R. M. Hill, J. Mater. Sci. **17**, 3630 (1982).
[50]K. L. Ngai, A. K. Jonscher, and C. T. White, Nature (London) **277**, 185 (1979).
[51]R. M. Hill, Phys. Status Solidi B **103**, 319 (1981).
[52]S. Havriliak and S. Negami, J. Polym. Sci. C **14**, 99 (1966).
[53]L. A. Dissado, R. R. Nigmatullin, and R. M. Hill, Adv. Chem. Phys. **63**, 253 (1985).
[54]D. W. Davidson and R. H. Cole, J. Chem. Phys. **19**, 1484 (1951).
[55]M. W. G. Whittall and G. A. Gehring, J. Phys. C **20**, 1619 (1987).
[56]S. Clough, Physica B + C **136B**, 145 (1986).
[57]S. Clough, P. J. McDonald, and F. O. Zelaya, J. Phys. C **17**, 4413 (1984).
[58]J. Kowalewski and T. Liljefors, Chem. Phys. Lett. **64**, 170 (1979).
[59]N. L. Owen, in *Internal Rotation in Molecules,* edited by W. J. Orville-Thomas (Wiley, New York, 1974), p. 157.
[60]P. A. Beckmann, C. I. Ratcliffe, and B. A. Dunell, J. Magn. Reson. **32**, 391 (1978).
[61]R. M. Fuoss and J. G. Kirkwood, J. Am. Chem. Soc. **63**, 385 (1941).
[62]*Modern Aspects of the Vitreous State,* edited by J. D. Mackenzie (Butterworths, London, 1960).